$$\eta = -\delta a \frac{3}{2}\left(\frac{k}{(e^2-1)a^3}\right)^{1/2}(1+e\cos f)(t-\tau) - \delta e\, a \sin f \frac{(2+e\cos f)}{1+e\cos f} - \delta\tau\left(\frac{k}{(e^2-1)a}\right)^{1/2}\times (1+e\cos f) + \delta\omega\frac{a(e^2-1)}{1+e\cos f} \quad (13)$$

4. Parabolic Orbits

In treating the perturbations about a parabolic orbit, one notes that one cannot simply let $e \to 1$ in (6) and (7), due to the divisors $1 - e^2$; and, moreover, $a \to \infty$. However, the quantity $a(1 - e^2)$ remains bounded and frequently is denoted by $2p$. In order to rearrange the previous results to read in terms of p, one notes that $\delta a(1 - e^2) = 2\delta p + 2ae\,\delta e$. However, for the parabolic case one may write $e = 1 + \epsilon$, $\delta e = \epsilon$, and $1 - e^2 = -2\epsilon + 0(\epsilon^2)$, so that $\delta a(1 - e^2) = 2\delta p - 2p(1 + \epsilon)$. Reformulating (6) and (7) in this fashion and retaining terms of $0(\delta p)$ and $0(\epsilon)$ in place of $0(\delta a)$ and $0(\delta e)$ for the elliptic orbit, one arrives at

$$\xi = \delta p\left\{\frac{2-\frac{3}{2}\sin^2 f}{1+\cos f} - \frac{1}{2}\sin^2 f\frac{(1-\cos f)}{(1+\cos f)^2}\right\} + \epsilon p\left\{-\frac{3}{2}(1-\cos f) + \frac{2(1+2\cos f)}{(1+\cos f)^2} + \frac{3}{10}\frac{(1-\cos f)^3}{(1+\cos f)^2}\right\} - \delta\tau\left(\frac{k}{2p}\right)^{1/2}\sin f \quad (14)$$

$$\eta = -\delta p\frac{3}{2}\sin f\left\{1+\frac{1}{3}\frac{1-\cos f}{1+\cos f}\right\} + \epsilon p\frac{3}{2}\sin f\left\{-\frac{2+\cos f}{1+\cos f} + \frac{\cos f - \frac{1}{3}}{(1+\cos f)^2} + \frac{1}{5}\left(\frac{1-\cos f}{1+\cos f}\right)^2\right\} - \delta\tau\left(\frac{k}{2p}\right)^{1/2}(1+\cos f) + \frac{\delta\omega\, 2p}{1+\cos f} \quad (15)$$

It is evident that one could have obtained the same results by applying the appropriate manipulations to (12) and (13), i.e., by working from the hyperbolic case.

From the definition of ϵ, it is also clear that $\epsilon > 0$ implies a perturbation toward hyperbolic orbits and for $\epsilon < 0$ toward elliptic ones.

5. Applications

As stated in the introduction, the results (6, 7, and 11–15), together with the special cases for $f_0 = 0$ (pericenter) or $f_0 = \pi$ (apocenter), are applicable whenever it is desired to exhibit the departures from an intended orbit due to faulty guidance or orbit determination at some point f_0. Taking the manned lunar mission as an example, one can trace the use of such formulas through its various phases.

Beginning with the coast trajectory that precedes the injection to the parking orbit, one may use (6, 7, and 11) to predict the departures from the nominal position and velocity at the injection point due to perturbations at the termination of launch burn. Next, the special case of these formulas for $e = 0$ [formulas (17–19) of Ref. 1] is useful in exhibiting the response of the parking orbit to errors at injection and, specifically, the discrepancies in position and velocity just prior to launch into the "translunar" phase.

Subsequent to this launch and any of the scheduled midcourse maneuvers, one can use (6, 7, and 11) or (14, 15, and 11) to predict the effects of a guidance error on the lunar approach. In fact, formulas (14) and (15) generally will be preferable to (6) and (7) for near-parabolic orbits (frequently encountered in lunar transfer trajectories) where (6) and (7) begin to lose accuracy. During the lunar approach, a high-precision position determination from the earth can be reduced to position and velocity errors at the last guidance maneuver by means of (14, 15, and 11). This would serve as a summary check on the guidance through midcourse.

After the transition to a lunar parking orbit, the case $e \simeq 0$ prevails again. If the ballistic descent to the lunar surface follows a Hohmann arc one has $f_0 = \pi$, and for the ascent to a return rendezvous in the lunar parking orbit the case $f_0 = 0$ very nearly applies. For the final approach in this rendezvous, the relative motion between the two vehicles can be described in detail by means of (17–19) of Ref. 1. These expressions are simple enough for on-board calculations of corrective maneuvers.

For the earth-bound trajectory from the moon, the earlier remarks on the translunar phase are again applicable. Finally, the expressions (6, 7, and 11) can be used to represent the spread between the high-altitude portions of re-entry trajectories in response to guidance forces exerted at the beginning of this phase. This is especially true for the skip trajectory that may have to be flown in order to reach an alternative landing site. In all of these approach maneuvers the forementioned formulas are helpful during the early part of re-entry, before the aerodynamic forces become comparable to the gravitational attraction.

References

[1] Geyling, F. T., "Satellite perturbations from extraterrestrial gravitation and radiation pressure," J. Franklin Inst. **269**, 375–407 (May 1960).

[2] Geyling, F. T., "Drag displacements and decay of near-circular satellite orbits," IXth Intern. Astronaut. Congr., Stockholm (1960); also submitted to AIAA J.

[3] Wisneski, M. L., "Error matrix for flight on a circular orbit," ARS J. **32**, 1416–1418 (1962).

Approximate Method for Hypersonic Nonequilibrium Blunt Body Airflows

D. Ellington*
Computing Devices of Canada Ltd., Ottawa, Ontario, and Canadian Armament Research and Development Establishment, Valcartier, Quebec

THE problems of hypersonic airflow including chemical effects have received much attention recently.[1] The inclusion of coupled rate chemistry in the analysis of shock layer flow behind detached shocks has been studied by Hall et al.,[2] who have developed an exact method of solution following the approach of Lick.[3] Starting with a specified bow shock, a numerical integration technique is employed to compute conditions at lattice points within the shock layer, specific streamline shapes being determined from mass flow integrals. The procedure is necessarily involved and demands solution by means of a large high-speed digital computer.

Several approximate methods have been reported of which the streamtube method[4, 5] and the shock-mapping method[6] may be mentioned. In the streamtube method the procedure is iterative, an assumed bow shock shape and location and an assumed pressure distribution being improved in successive iterations in real gas flow using continuity equations until a self-consistent solution is obtained. In shock-mapping,

Received December 23, 1962; revision received June 10, 1963. This work was administered by the Aerophysics Wing, Canadian Armament Research and Development Establishment and was supported partly by the Advanced Research Projects Agency under Order 133. The author is grateful to B. K. Winterbon, D. A. Keeley, and P. Sefton for various helpful suggestions.

* Research Scientist, Aerophysics Wing.

an integral transform is employed to establish a correspondence between normal shock and blunt body flows. The correspondence applies in situations for which binary kinetics govern the chemistry and for which Newtonian theory is applicable. Under these conditions, good agreement is found with exact calculations, especially if the assumed pressure distribution is taken from the corresponding exact calculation, the flow velocity being assumed constant along streamlines. Streamline and body locations are determined from mass flow relations as usual.

In this note, a relatively simple, noniterative, direct, approximate method is described for determining the chemical and thermodynamic state along streamlines in the shock layer and the simultaneous location of the streamlines and shock relative to the body. The method used is an extension of that due to Freeman,[7] the chemical model comprising a mixture of three Lighthill ideal dissociating gases,[8] viz., N_2, O_2, and NO, together with the atomic species N and O. The assumption of a mixture of Lighthill gases implies that the average vibrational temperatures of the molecular species are the same and are one-half of the average translational temperature of the mixture. Electronic excitation-ionization and vibration-dissociation couplings are not considered. The chemical reactions proceeding between the species are chosen as the dominant ones in the system of innumerable reactions which proceed in air at higher temperatures[9]:

$$M + O_2 \underset{k_1}{\overset{k_1'}{\rightleftharpoons}} 2O + M$$

$$M + N_2 \underset{k_2}{\overset{k_2'}{\rightleftharpoons}} 2N + M$$

$$NO + O \underset{k_3}{\overset{k_3'}{\rightleftharpoons}} N + O_2$$

$$N_2 + O \underset{k_4}{\overset{k_4'}{\rightleftharpoons}} NO + N$$

$$M + NO \underset{k_5}{\overset{k_5'}{\rightleftharpoons}} N + O + M$$

$$N_2 + O_2 \underset{k_6}{\overset{k_6'}{\rightleftharpoons}} 2\,NO$$

M is any one of the five reacting species, and k_i', k_i are the forward and reverse rate constants, respectively, given by

$$k_i' = c_i T^{-s_i} \exp(-D_i/kT) \qquad k_i = c_i T^{-s_i} f_i(T)$$

where c_i, s_i, D_i, k are constants, and where $f_i(T)$ can be obtained from statistical thermodynamics[10, 11] or from experimental determinations.[12]

The specific internal energy u of the gas mixture comprising three ideal dissociating gases is

$$u = \frac{3k}{2m} T + \frac{D_{N_2}}{4m} (2\alpha_N + \alpha_{NO}) + \frac{D_{O_2}}{4m} (2\alpha_O + \alpha_{NO}) - \frac{D_{NO}}{2m} \alpha_{NO}$$

where D_{N_2}, D_{O_2}, D_{NO} are dissociation energies per molecule, α_N, α_O, α_{NO} are mass fractions, and m is the mass of the oxygen or nitrogen atom (assumed equal). The equation of state is

$$p = (k/2m)\rho T(1 + \alpha_N + \alpha_O)$$

from which follows the expression for specific enthalpy:

$$i = u + \frac{p}{\rho} = \frac{kT}{2m} (4 + \alpha_N + \alpha_O) + \frac{1}{4m} \times \{D_{N2}(2\alpha_N + \alpha_{NO}) + D_{O2}(2\alpha_O + \alpha_{NO}) - 2D_{NO}\alpha_{NO}\} \quad (1)$$

In the notation of Fig. 1, the equations describing the steady flow of inviscid fluid in the shock layer, neglecting transport effects, are as follows:

Continuity

$$\frac{\partial}{\partial\theta} (\rho u_\theta r \sin\theta) + \frac{\partial}{\partial r} (\rho u_r r^2 \sin\theta) = 0 \quad (2)$$

Momentum

$$\frac{u_\theta}{r} \frac{\partial u_\theta}{\partial\theta} + u_r \frac{\partial u_\theta}{\partial r} + \frac{u_\theta u_r}{r} + \frac{1}{\rho r} \frac{\partial p}{\partial\theta} = 0 \quad (3)$$

$$\frac{u_\theta}{r} \frac{\partial u_r}{\partial\theta} + u_r \frac{\partial u_r}{\partial r} - \frac{u_\theta^2}{r} + \frac{1}{\rho} \frac{\partial p}{\partial r} = 0 \quad (4)$$

Energy

$$\frac{u_\theta}{r} \frac{\partial i}{\partial\theta} + u_r \frac{\partial i}{\partial r} - \frac{u_\theta}{\rho r} \frac{\partial p}{\partial\theta} - \frac{u_r}{\rho} \frac{\partial p}{\partial r} = 0 \quad (5)$$

Subject to the assumptions of large local density in the shock layer and small density gradient along the body compared with that normal thereto, Freeman[13] has shown that to a first approximation u_θ and i are constant along streamlines and are given by

$$u_\theta \simeq U_\infty \sin\xi \qquad i \simeq \tfrac{1}{2} U_\infty^2 \cos^2\xi$$

Introducing a stream function ψ to satisfy the continuity equation, defined by

$$\partial\psi/\partial r = \rho u_\theta r \sin\theta \qquad \partial\psi/\partial\theta = -\rho u_r r^2 \sin\theta \quad (6)$$

it may be shown that, at the shock, $\psi = \frac{1}{2}\rho_\infty U_\infty r^2 \sin^2\theta$, which Freeman approximates as

$$\psi \simeq \tfrac{1}{2}\rho_\infty U_\infty a^2 \sin^2\xi \quad (7)$$

throughout the shock layer.

Neglect of the first two terms of the second momentum equation, Eq. (4), leads to

$$p(\psi) = p_s(\theta) + \frac{1}{\sin\theta} \int_{\psi_s}^{\psi} \frac{u_\theta}{r^2} d\psi$$

where suffix s refers to conditions immediately downstream of the shock. This form, together with the first-order ap-

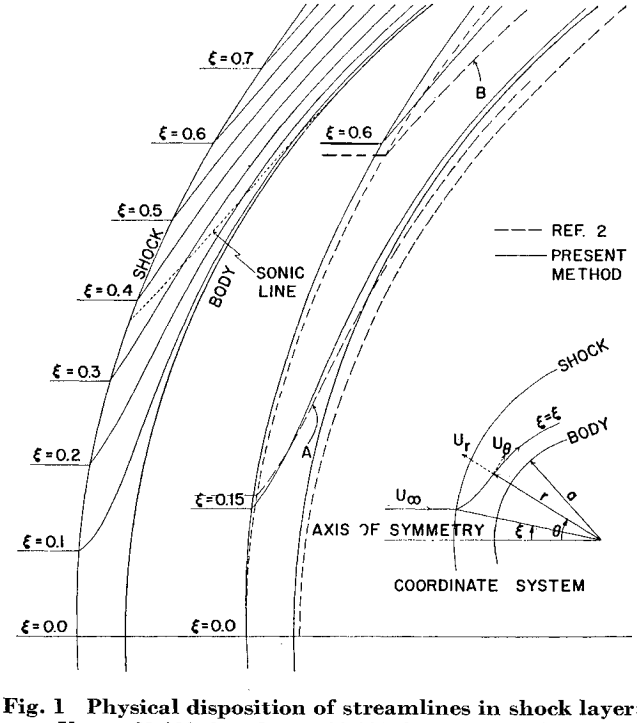

Fig. 1 Physical disposition of streamlines in shock layer; U = 23,000 fps, h = 200,000 ft, a = 0.065 ft.

proximations for ψ and u_θ, yields Freeman's expression for the pressure in the shock layer,

$$p(\theta,\xi) = \left\{\frac{\sin 3\theta + \sin^3\xi}{3\sin\theta}\right\}\rho_\infty U_\infty^2 \qquad (8)$$

It is now possible to develop a second approximation for u_θ by retaining the term $(1/\rho r)(\partial p/\partial\theta)_r$ in the first momentum equation, Eq. (3). In differential form, one obtains

$$\left(\frac{\partial u_\theta}{\partial\theta}\right)_\xi = \frac{\rho_\infty U_\infty^2}{3\rho u_\theta}\frac{\cos\theta}{\sin^2\theta}(8\sin^3\theta + \sin^3\xi) \qquad (9)$$

with $u_\theta = U_\infty \sin\xi$ as an initial condition at the shock. The specific enthalpy i now may be expressed to a second approximation as

$$i = \tfrac{1}{2}(U_\infty^2 - u_\theta^2) \qquad (10)$$

From Eqs. (1) and (10), the local temperature T may be expressed simply in terms of u_θ and the mass fractions. The local density ρ then follows from the equation of state together with Eq. (8). With the assumption

$$(d/dt)(\ ) \simeq (u_\theta/a)\{(\partial/\partial\theta)(\ )\}_\xi \qquad (11)$$

throughout the shock layer, the five chemical rate equations for the mass fractions together with Eq. (9) constitute six total differential equations connecting the five mass fractions and u_θ as dependent variables, with θ as independent variable and ξ as parameter. These equations may be solved numerically for each streamline $\xi = \xi$ by a forward integration technique. The physical disposition of the streamlines in the shock layer is obtained from the streamline solutions, the value of r corresponding to each (θ,ξ) point being obtained by integration over the shock layer using the result

$$r^2 = a^2\left[1 + \frac{\rho_\infty U_\infty}{\sin\theta}\int_0^\xi \frac{\sin 2\xi}{\rho u_\theta}\,d\xi\right]$$

which follows from Eq. (6) written in the form

$$\int_a^r r\,dr = \int_0^\psi \frac{d\psi}{\rho u_\theta \sin\theta}$$

by substitution from Eq. (7).

The foregoing scheme of solution may be executed simply with the aid of a small digital computer.[14] It should be noted that the method fails for streamlines close to the axis of symmetry since approximation (11) is inadequate. Conditions along these streamlines, however, can be obtained by extrapolation of the results to $\xi = 0$. A further difficulty with the method is encountered at $\theta = \pi/3$ on the body, at which point the pressure p approaches zero according to the Newtonian

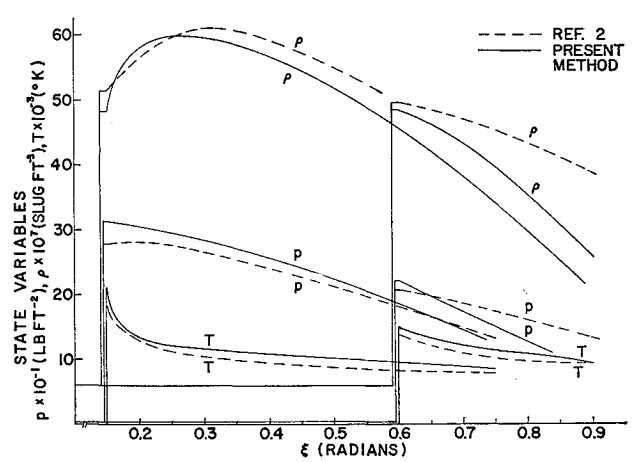

Fig. 2 Thermodynamic state along $\xi = 0.15$ and $\xi = 0.60$ streamlines; U_∞ = 23,000 fps, h = 200,000 ft, and a = 0.065 ft.

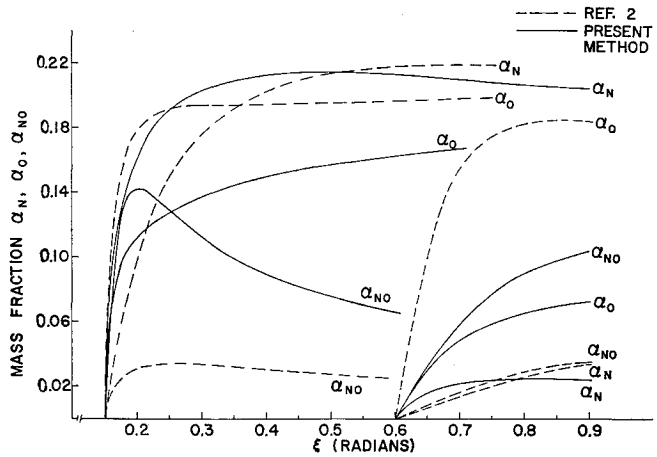

Fig. 3 Chemical composition along $\xi = 0.15$ and $\xi = 0.6$ streamlines; U_∞ = 23,000 fps, h = 200,000 ft, a = 0.065 ft.

expression. At moderate hypersonic Mach numbers, however, the sonic line is contained within the region of θ somewhat less than $\pi/3$, so that a characteristics solution for this reacting mixture of gases can be initiated before the divergences due to the zero in the pressure distribution are reached.[11]

Typical results for the case of a sphere of 0.065-ft radius, traveling at 23,000 fps at an altitude of 200,000 ft, are shown in Figs. 1–3. Numerical integration of the equations was performed[14] using a Runge-Kutta technique with the initial conditions $\alpha_N = 0$, $\alpha_O = 0$, $\alpha_{NO} = 0$, $\alpha_{O_2} = 0.2$, $\alpha_{N_2} = 0.8$, and $u_\theta = U_\infty \sin\xi$ at the shock, and with rate constants as detailed by Wray.[12] The results may be compared with an exact solution obtained by Hall et al.[2] for a catenary shock of 0.0692-ft axial radius of curvature. In spite of the slightly different bow shock geometries, the locations and shapes of the two bodies and corresponding streamlines are quite similar (Fig. 1). The thermodynamic state along two typical streamlines, A and B of Ref. 2, is seen to compare well between the two methods (Fig. 2). The slightly different conditions immediately behind the shock result from different assumptions regarding the degree of vibrational excitation realized there. The chemical state along the same two streamlines is shown and compared in Fig. 3. The higher NO overshoot, characteristic of shock-heated air,[15] indicated in the case of the approximate solution, arises as a result of the inclusion of the reaction $N_2 + O_2 \rightleftharpoons 2NO$ in the present calculations. For the same reason the initial rate of increase of the mass fraction of atomic oxygen is suppressed in the present solution. Nevertheless, the comparison shows the usefulness of the approximate method in investigating the effects of rate chemistry including recombination reactions. As noted by Hall et al.,[2] the boundary-layer thickness for the flight conditions currently considered would be about one-half of the shock stand-off distance, but this fact does not enter into the present considerations, which are concerned solely with testing the usefulness of the approximate inviscid flow method.

References

[1] Cheng, H. K., "Recent advances in hypersonic flow research," AIAA J. 1, 295–310 (1963).

[2] Hall, H. G., Eschenroeder, A. Q., and Marrone, P. V., "Blunt-nose inviscid airflows with coupled non-equilibrium processes," J. Aerospace Sci. 29, 1038–1051 (1962).

[3] Lick, W., "Inviscid flow of a reacting mixture of gases around a blunt body," J. Fluid Mech. 7, 128–144 (1960).

[4] Vaglio-Laurin, R. and Bloom, M. H., "Chemical effects in external hypersonic flows," *Hypersonic Flow Research*, edited by F. R. Riddell (Academic Press, New York, 1962), pp. 205–254.

[5] Lin, S. C. and Teare, J. D., "A streamtube approximation for calculations of reaction rates in the inviscid flow field of hypersonic objects," Avco Everett Res. Lab. RN 223 (August 1961).

[6] Gibson, W. E. and Marrone, P. V., "Correspondence between normal-shock and blunt-body flows," Phys. Fluids **5**, 1649–1656 (1962).

[7] Freeman, N. C., "Non-equilibrium flow of an ideal dissociating gas," J. Fluid Mech. **4**, 407–425 (1958).

[8] Lighthill, M. J., "Dynamics of a dissociating gas. Part I. Equilibrium flow," J. Fluid Mech. **2**, 1–32 (1957).

[9] Ludwig, C. B., "Chemical kinetics behind strong shock waves. II—Review of chemical reactions occurring in an N_2-O_2 mixture at 6000 to 10,000°K," General Dynamics Convair Phys. Rept. ZPh-050 (December 1959).

[10] Fowler, R. and Guggenheim, E. A., *Statistical Thermodynamics* (Cambridge University Press, Cambridge, 1952), Chap. 3, p. 97.

[11] Ellington, D. and Winterbon, B. K., "On the development of a method for predicting the gaseous radiation characteristics of blunt bodies at hypersonic speeds. Part 1. Chemical kinetics and gas dynamics," Canadian Armament Res. Dev. Establ. Tech. Memo. 627/61 (November 1961).

[12] Wray, K. L., "Chemical kinetics of high temperature air," *Hypersonic Flow Research*, edited by F. R. Riddell (Academic Press, Inc., New York, 1962), pp. 181–204.

[13] Freeman, N. C., "On the theory of hypersonic flow past plane and axially symmetric bluff bodies," J. Fluid Mech. **1**, 366–387 (1956).

[14] Ellington, D. and Keeley, D. A., "On the development of a method for predicting the gaseous radiation characteristics of blunt bodies at hypersonic speeds. Part 2—IBM 1620 digital computer program for flow field solution in shock cap," Canadian Armament Res. Dev. Establ. Tech. Memo. 726/63 (February 1963).

[15] Wray, K. L. and Teare, J. D., "A shock tube study of the kinetics of nitric oxide at high temperatures," Avco Everett Res. Lab. RR 95 (June 1961).

Area-Integrated Heat Rates for Several Axisymmetric Vehicles

H. G. Myer* and A. Ambrosio†
Space Technology Laboratories Inc., Redondo Beach, Calif.

Averaging coefficients that allow rapid estimates of area-integrated heat rates are determined for some configurations of practical interest. The values of these averaging coefficients lie in the range from 0.68 to 1.00.

Nomenclature

A = area
h = specific enthalpy
K = averaging coefficient defined by Eq. (1)
K' = averaging coefficient defined by Eq. (2)
P = pressure
q = heating rate per unit area
q_t = heating rate, integrated over surface area
r = radial distance
R = radius
s = wetted distance measured along body surface
u = velocity
γ = ratio of specific heats
θ_c = cone half-angle
θ_s = body angle, measured between local radius vector and the tangent to the surface
μ = coefficient of viscosity
ρ = density

Subscripts

δ = edge of boundary layer
0 = stagnation
∞ = freestream
B = base of body
N = nose

IN the initial stages of entry vehicle preliminary design, it is very advantageous to be able to perform rapid estimates of the area-integrated heat rates. From these estimates, decisions can be made regarding vehicle configurations and the corresponding heat protection systems to be investigated.

This may be accomplished by relating the desired heat rate to stagnation point heat rate and vehicle base area through an averaging coefficient. That is,

$$q_t = KA_Bq_0 \tag{1}$$

For some vehicle shapes, it is convenient to introduce the ratio of nose radius to base radius into the equation for the desired heat rate:

$$q_t = K'(R_N/R_B)^{1/2}A_Bq_0 \tag{2}$$

If the values of K or K' are known, total heat rates are computed easily from either Eq. (1) or (2).

To determine the values of K and K', Eqs. (1) and (2) are inverted to read

$$K = q_t/A_Bq_0 \tag{3}$$

and

$$K' = \frac{q_t}{(R_N/R_B)^{1/2}\ A_Bq_0} \tag{4}$$

The equation for laminar heat rate at any point on an axisymmetric vehicle may be expressed as[1]

$$q = f(u_\infty,\rho_0,\mu_0,h_0)R_B^{-1/2}\,F(r/R_B) \tag{5}$$

where

$$F\left(\frac{r}{R_B}\right) = \frac{(r/R_B)\left[(P_\delta/P_0)^{(\gamma+1)/\gamma} - (P_\delta/P_0)^2\right]^{1/2}}{\left\{\int_0^{r/R_B}(r/R_B)^2\left[(P_\delta/P_0)^{(\gamma+1)/\gamma} - (P_\delta/P_0)^2\right]^{1/2}\left[d(r/R_B)/\cos\theta\right]\right\}^{1/2}} \tag{6}$$

At the stagnation point of an axisymmetric vehicle, Eq. (6) is reduced to

$$F_0 = 2(R_B/R_N)^{1/2}[(\gamma-1)/\gamma]^{1/4} \tag{7}$$

The integral of Eq. (5) taken over the surface of the vehicle gives total heat rate so that, with the aid of Eq. (5), Eq. (3) becomes

$$K = \left(\frac{2}{F_0}\right)\int_0^1\left(\frac{r}{R_B}\right)F\,\frac{d(r/R_B)}{\cos\theta} \tag{8}$$

Substitution of Eqs. (6) and (7) into Eq. (8) results in

$$K = \left(\frac{R_N}{R_B}\right)^{1/2}\left(\frac{\gamma}{\gamma-1}\right)^{1/4}\int_0^1 \frac{(r/R_B)^2\left[(P_\delta/P_0)^{(\gamma+1)/\gamma} - (P_\delta/P_0)^2\right]^{1/2}\left[d(r/R_B)/\cos\theta\right]}{\left\{\int_0^{r/R_B}(r/R_B)^2\left[(P_\delta/P_0)^{(\gamma+1)/\gamma} - (P_\delta/P_0)^2\right]^{1/2}\left[d(r/R_B)/\cos\theta\right]\right\}^{1/2}} \tag{9}$$

Received January 14, 1963.

* Member of the Technical Staff, Aerodynamics Department.

† Staff Engineer to Aerosciences Laboratory Director.